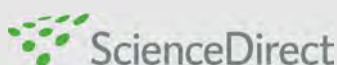
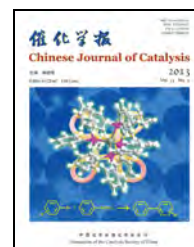


available at www.sciencedirect.comjournal homepage: www.elsevier.com/locate/chnjc

Article

Role of ReO_x in Re-modified Rh/ZrO_2 and Ir/ZrO_2 catalysts in glycerol hydrogenolysis: insights from first-principles study

Jing Guan^a, Xiufang Chen^a, Gongming Peng^a, Xicheng Wang^a, Quan Cao^a, Zhenggang Lan^{a,b,*}, Xindong Mu^{a,#}

^a Key Laboratory of Biobased Materials, Qingdao Institute of Bioenergy and Bioprocess Technology, Chinese Academy of Sciences, Qingdao 266101, Shandong, China

^b The Qingdao Key Lab of Solar Energy Utilization and Energy Storage Technology, Qingdao Institute of Bioenergy and Bioprocess Technology, Chinese Academy of Sciences, Qingdao 266101, Shandong, China

ARTICLE INFO

Article history:

Received 20 April 2013

Accepted 20 May 2013

Published 20 September 2013

Keywords:

Density functional theory

Glycerol hydrogenolysis

Propanediol

Re-modified

Metal catalyst

Thermodynamics

ABSTRACT

The thermodynamics of glycerol hydrogenolysis to produce 1,2-propanediol (1,2-PDO) and 1,3-propanediol (1,3-PDO) over Ru/ZrO_2 , Rh/ZrO_2 , $\text{ReO}_x\text{-Rh}/\text{ZrO}_2$, and $\text{ReO}_x\text{-Ir}/\text{ZrO}_2$ were studied using density functional theory calculations, with a special focus on the mechanism controlling the activity and selectivity of the reactions. It is found that the decomposition of glycerol on Ru/ZrO_2 and Rh/ZrO_2 proceeds through a dehydration-hydrogenation mechanism. The formation of 1,2-PDO is thermodynamically favored, and the activity of the Ru-based catalyst is higher than that of the Rh-based one. In contrast, a direct hydrogenolysis mechanism is proposed for the Re-modified Rh and Ir catalysts, in which a dissociated H atom on the $\text{Rh}(\text{Ir})$ metal surface attacks the C–O bond neighboring the alkoxide species on the ReO_x cluster. In the presence of $\text{ReO}_x\text{-Rh}/\text{ZrO}_2$, the modified catalyst favors the production of 1,2-PDO, and 1,3-PDO production becomes competitive. However, the $\text{ReO}_x\text{-Ir}/\text{ZrO}_2$ catalyst significantly improves 1,3-PDO selectivity. The direct hydrogenolysis pathway, as opposed to the indirect hydrogenolysis mechanism for monometallic catalysts, may be the key to the high 1,3-PDO selectivity on the modified catalysts, where the hydroxylated Re group facilitates the formation of terminal alkoxide species rather than secondary alkoxides. Steric effects are important in preferential terminal alkoxide formation on the $\text{ReO}_x\text{-Ir}/\text{ZrO}_2$ catalysts because of the growth of large Ir-Re clusters, resulting in high selectivity for 1,3-PDO.

© 2013, Dalian Institute of Chemical Physics, Chinese Academy of Sciences.

Published by Elsevier B.V. All rights reserved.

1. Introduction

Glycerol, which is a major byproduct in biodiesel manufacturing processes, has been identified by the U.S. Department of Energy as one of the top 12 building block chemicals in the biorefinery industry [1]. It is therefore necessary to develop

new applications of glycerol to make biodiesel production a cost-effective process. This has triggered intensive research into the conversion of glycerol to high-value bio-based chemicals or materials. Among the various processes for converting glycerol to marketable chemicals, glycerol hydrogenolysis to propanediols has attracted significant interest. It is well known

* Corresponding author. Tel: +86-532-80662630; Fax: +86-532-80662778; E-mail: lanzg@qibebt.ac.cn

Corresponding author. Tel: +86-532-80662723; Fax: +86-532-80662724; E-mail: muxd@qibebt.ac.cn

This work was supported by the Natural Science Foundation of Shandong Province (ZR2010BQ001), the National Natural Science Foundation of China (21273260, 21201174 and 21103213), 100 Talents Program of the Chinese Academy of Sciences, and the Director Innovation Foundation of Chinese Academy of Sciences-Qingdao Institute of Bioenergy and Bioprocess Technology.

DOI: 10.1016/S1872-2067(12)60626-3 | <http://www.sciencedirect.com/science/journal/18722067> | Chin. J. Catal., Vol. 34, No. 9, September 2013

that many value-added products, such as 1,2-propanediol (1,2-PDO) and 1,3-propanediol (1,3-PDO), can be directly obtained from glycerol hydrogenolysis via catalytic deoxygenation [2].

A number of heterogeneous catalysts, ranging from normal metal-based Cu [3–5] and Ni [6,7] catalysts to noble-metal-based Ru [8–11], Rh, Pt, Pd, Ir, and Au [12–15] catalysts, have been studied to check their catalytic abilities in the hydrogenolysis of glycerol to PDOs. The main challenge in the hydrogenolysis of glycerol is to control the branching ratio between 1,2-PDO and 1,3-PDO, which requires highly selective cleavage of the primary or secondary hydroxyl groups in glycerol. Undoubtedly, the selectivity for the final product strongly depends on the catalyst. Considerable research has therefore been conducted to find effective catalytic systems that can discriminate between, and selectively break, the two C–O bonds of glycerol. Because cleavage of the primary hydroxyl group is easier, for steric reasons, significant advances have been made in achieving high-yield conversion of glycerol to 1,2-PDO using supported Cu, Ru, and Rh catalysts. The direct deoxygenation of glycerol to the more valuable 1,3-PDO is more challenging because it suffers from very low yields. However, it has recently been reported that Rh-/Pt-based catalysts combined with a W-based cocatalyst or modifier provide a promising way of transforming glycerol to 1,3-PDO [4,15–19]. Chaminand et al. [4] reported the production of 1,3-PDO using a catalyst system containing Rh/C and H_2WO_4 . Shinmi et al. [16,17] demonstrated that the addition of a second metal (Re, Mo, or W) to Rh/ SiO_2 enhances conversion to 1,3-PDO in aqueous solutions. In particular, the formation of 1,3-PDO was significantly promoted by modification of the catalyst with Re. Recently, the same authors increased the 1,3-PDO selectivity to 65% using a Re-modified Ir/ SiO_2 catalyst. They also proposed that a reported reaction via a Re-based catalyst followed a similar mechanism [18,19].

Understanding the reaction mechanism is the first step in the rational design of catalysts. Several mechanisms have been proposed for glycerol hydrogenolysis reduction to propanediols. The widely accepted mechanism involves dehydration-hydrogenation [4,5] or dehydrogenation-dehydration-hydrogenation schemes [20,21]. In contrast, direct hydrogenolysis of C–O bonds has been postulated for Re-modified Rh and Ir catalysts; this is strongly supported by experimental evidence [16–18]. A common feature of these catalysts is the existence of low-valent ReO_x clusters directly bonded to the metal sites. It has been proposed that one of the glycerol oxygen atom is initially anchored to a hydroxyl group on Re. The produced alkoxide species acts as an acceptor in the following hydride transfer, forming 1,2-PDO or 1,3-PDO. The branching ratio of the products depends on which hydroxyl group of glycerol is adsorbed and which one is cleaved. The Rh- ReO_x and Ir- ReO_x interfaces would be the locations of the active sites [17].

Despite this growing body of experimental work, a systemic understanding of the reaction mechanisms governing the rates and selectivities of C–O bond scissions over these interesting catalysts remains elusive. It is therefore essential to obtain a detailed theoretical understanding of the reaction mechanisms. Density functional theory (DFT) calculations have been exten-

sively used to gain fundamental insights into catalytic reaction mechanisms, but only a few studies have been carried out to clarify glycerol conversions to propanediols on metallic catalysts at the fundamental level because of the complexity of the reactions. So far, no generally accepted mechanism has been reported in the literature [22–25]. Various dehydration mechanisms of neutral and protonated glycerols were investigated by Nimols et al. [22] using quantum mechanical calculations. It was found that the addition of acids facilitates the loss of the primary or central hydroxyl group via hydride transfer or substitution reaction mechanism. Coll et al. [24] represented the thermodynamic profiles of the dehydration of glycerol at the surfaces of Ni(111), Rh(111), and Pd(111) by DFT studies. The dependence of the intermediate stability on the metal provides a useful clue in designing new catalysts for selective 1,3-PDO formation. Recently, Dumesic's research group [25] combined DFT calculations and experimental observations to examine the hydrogenolysis of cyclic ethers and polyols on ReO_x -doped noble-metal catalysts. They confirmed the preferential formation of an intermediate oxocarbenium cation through protonation of acidic surface Re-OH groups, which ensures a high yield of 1,3-PDO.

In this study, we used theoretical DFT calculations to investigate glycerol hydrogenolysis to produce 1,2-PDO and 1,3-PDO on supported $\text{Re}_2\text{O}_3\text{H}_2$ -Rh₄ and $\text{Re}_2\text{O}_3\text{H}_2$ -Ir₄ clusters, with the aim of identifying plausible reaction mechanisms and understanding the bifunctional role of ReO_x -modified catalysts in this process. Based on the extensive experiments carried out by Tomishige's group [16–18], the direct hydrogenolysis mechanism for glycerol over Rh(Ir)- ReO_x is examined in this work. To the best of our knowledge, no systematic theoretical study of the direct hydrogenolysis mechanism has been reported. In our previous work [26], ZrO_2 was used to identify the origin of the effect of the oxidic support on the reactivity of Cu-based catalysts in glycerol hydrogenolysis; the use of a ZrO_2 support gave good selectivity for propanediols because of the optimum acidity of this catalytic material [14]. For completeness, investigations on Ru₄ and Rh₄ were included for comparison in the present work. As a first step towards this goal, we identified possible reaction mechanisms on different catalysts from the thermodynamics point of view. The decisive role of ReO_x in improving the catalytic activity and 1,3-PDO selectivity with respect to monometallic clusters was qualitatively addressed by examining all the critical geometries and energetics of the catalysts, adsorbates, and intermediates. Our findings provide a preliminary understanding of the regioselectivity in the deoxygenation of biomass-derived feedstocks over bifunctional catalysts in the presence of effective hydroxylated Re species.

2. Methods and models

2.1. Computational method

Plane-wave DFT calculations with the projector-augmented wave method were carried out as implanted in the Vienna ab initio simulation package (VASP) [27–30]. The generalized gradient approximation with the Perdew-Wang exchange-correla-

tion functional (GGA-PW91) was used [31]; this has been shown to work well for surfaces. The kinetic energy cutoff for a plane-wave basis set was 400 eV. We applied Monkhorst-Pack mesh k -points [32] of $(3 \times 3 \times 3)$ and $(3 \times 3 \times 1)$ for bulk and surface calculations, ensuring convergence of the whole system. Structural optimization was based on the conjugate gradient-minimization scheme, and spin-unrestricted calculations were also performed. The convergence of energy and forces were set to 1×10^{-4} eV and 0.3 eV/nm, respectively.

2.2. Surface models

To accommodate a metal cluster with small lateral interactions between periodic images, all surface reactions were modeled on a $c(3 \times 3)$ $\text{ZrO}_2(111)$ slab of thickness six atomic layers (see Fig. 1(a) and (b)), and a vacuum layer of thickness 1.5 nm to minimize electrostatic interactions between periodic images in the direction of the surface normal; this is sufficient to represent the geometric relaxation of zirconia surfaces [33]. In all simulations, the bottom three layers of the slab were held fixed at the bulk ZrO_2 lattice position, while the remaining three uppermost ZrO_2 layers, the monometallic and bimetallic clusters, and the adsorbates for reactivity studies were allowed to relax.

Ru_4 and Rh_4 clusters were chosen as the models supported on ZrO_2 surfaces in this work, as these are the smallest three-dimensional structures that provide both metal-metal and metal-support interactions [34–37]. Similar cluster models have been used for Rh_4 nanoparticles deposited on ZrO_2 and CeO_2 supports, and shown to be able to capture the chemistry of nanosized metal particles in catalytic reactions [36,37]. In our previous work, we studied the selective hydrogenolysis of glycerol on Cu_4 clusters dispersed on ZrO_2 and MgO . To examine the effect of cluster size on the calculation results, a larger model containing eight Cu atoms (Cu_8) was used. The calculation results indicated that Cu_8 clusters exhibited adsorption properties similar to those of Cu_4 clusters [26]. To study the effect of Re additives, $\text{Re}_2\text{O}_3\text{H}_2\text{-Rh}_4$ and $\text{Re}_2\text{O}_3\text{H}_2\text{-Ir}_4$ clusters were constructed on the ZrO_2 surface. In the model structures, one Re atom is adsorbed on the three-fold site of the metal cluster and the other one is located on the Rh–Rh (Ir–Ir) bridging sites. This is in accordance with the extended X-ray absorption fine structure (EXAFS) characterization results, which suggest that Re atoms tend to occupy the three-fold hollow site on the metal (111) surface [17]. In addition, the two Re atoms

are connected by one bridging oxygen atom, and each is bonded with one terminal hydroxyl group (Fig. 1(c) and (d)). The presence of Re–Rh (Re–Ir), Re–Re, and Re–OH bonds was confirmed by the Re L_3 -edge EXAFS spectra, and the computed bond lengths were in good agreement with the corresponding experimental values. According to this estimation, the average valence of Re in the model structure is calculated to be +2. Temperature-programmed reduction and EXAFS analysis also revealed that the Re was present as Re^{7+} on the calcined catalyst, whereas reductive pretreatment reduced Re to an oxidation state of Re^{2+} to $\text{Re}^{2.5+}$ [17].

In this work, we calculated the adsorption energies using the equation $E_{\text{ads}} = E(\text{surface} + \text{adsorbate}) - E(\text{surface}) - E(\text{adsorbate})$, where $E(\text{surface} + \text{adsorbate})$, $E(\text{surface})$, and $E(\text{adsorbate})$ denote the calculated electronic energies of the optimized adsorption configurations, the bare surface, and a free molecule, respectively. With this definition, a negative E_{ads} value implies that adsorption of molecules is thermodynamically favorable. The energy reference for each step is the clean slab plus the gas-phase energies of the reactants.

3. Results and discussion

3.1. Surfaces of $\text{Ru}_4/\text{ZrO}_2(111)-(3 \times 3)$, $\text{Rh}_4/\text{ZrO}_2(111)-(3 \times 3)$, $\text{Re}_2\text{O}_3\text{H}_2\text{-Rh}_4/\text{ZrO}_2(111)-(3 \times 3)$, and $\text{Re}_2\text{O}_3\text{H}_2\text{-Ir}_4/\text{ZrO}_2(111)-(3 \times 3)$

The optimized structures modeling the Ru and Rh tetramers (Ru_4 and Rh_4) anchored on the $\text{ZrO}_2(111)$ surface are shown in Fig. 1. For both tetramers, their minimum-energy geometries show planar structures instead of tetrahedral configurations, similar to gas-phase cases. We therefore take only planar geometries as the initial geometries in the discussion below. The equilibrium geometries of Rh_4 and Ru_4 clusters are distorted slightly after deposition on the ZrO_2 substrate. These clusters interact with the surface through all four metal atoms simultaneously, because it is possible to retain the Rh–Rh or Ru–Ru bonds. The same situation exists for Cu tetramers aggregated on $\text{ZrO}_2(111)$ and $\text{MgO}(100)$ surfaces; see our previous work [26]. In the $\text{Ru}_4/\text{ZrO}_2(111)-(3 \times 3)$ model structure (Fig. 1(a)), four Ru–O bonds are formed on adsorption, with an average length of 0.199 nm. In addition, three Ru–Zr bonds are formed, with an average distance of 0.281 nm. For the Rh_4 structure (Fig. 1(b)), the cluster-surface bonding scheme is slightly dif-

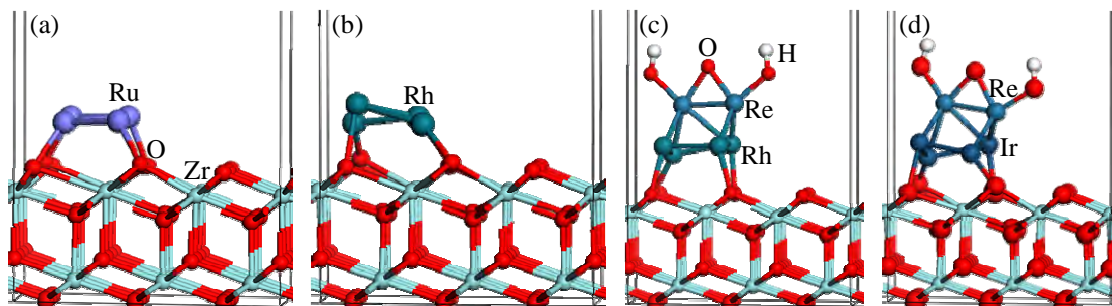


Fig. 1. Side views of optimized Ru_4 supported on $\text{ZrO}_2(111)$ surface in rhombic structure (a), Rh_4 supported on $\text{ZrO}_2(111)$ surface in rhombic structure (b), $\text{Re}_2\text{O}_3\text{H}_2$ -modified Rh_4 cluster supported on $\text{ZrO}_2(111)$ surface (c), and $\text{Re}_2\text{O}_3\text{H}_2$ -modified Ir_4 cluster supported on $\text{ZrO}_2(111)$ surface (d).

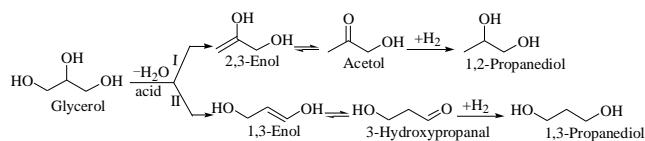
ferent. On relaxation, the structure is distorted to a bent rhombus, in which Rh atoms are alternately placed close to and away from the surface atoms. The shortest Rh–Zr and Rh–O bond distances are 0.261 and 0.201 nm, respectively.

The adsorption structures of $\text{Re}_2\text{O}_3\text{H}_2$ -modified Rh_4 and Ir_4 clusters on the ZrO_2 surface are illustrated in Fig. 1(c) and (d). The Rh_4 and Ir_4 clusters both maintain a planar frame on the ZrO_2 surface. The adsorbed Rh atom binds to the supporting lattice oxygen atoms, and the average Rh–O distance is 0.209 nm. In addition, two Re atoms are directly bonded to the bridging sites of Rh_2 , with Rh–Re and Re–Re distances of 0.234 and 0.246 nm, respectively. In the case of the relaxed $\text{Re}_2\text{O}_3\text{H}_2\text{-Ir}_4/\text{ZrO}_2(111)\text{-(}3 \times 3\text{)}$ structure, the Ir_4 cluster deviates only slightly from planarity. The average Ir–Ir and Ir–Re distances are 0.274 and 0.240 nm, respectively. For both systems, the predicted bond distances are consistent with the measured values obtained in EXAFS experiments [17]. This provides further evidence to support our model construction.

3.2. Hydrogenolysis of glycerol on $\text{Ru}_4/\text{ZrO}_2(111)$ surface: DFT studies

Scheme 1 shows the metal-catalyzed dehydration-hydrogenation routes that were observed over Cu-based and Ru-based catalysts under acidic conditions, leading to different products [4,5]. The branching ratio to produce 1,2-PDO and 1,3-PDO is highly dependent on which C–O bond dehydrated first. Primary C–O bond cleavage leads to formation of a 2,3-enol and then an acetol. Hydrogenation of the acetol gives 1,2-PDO. The formation of 1,3-PDO proceeds via 3-hydroxypropanal as an intermediate, which is formed after initial elimination of the secondary alcohol group of glycerol.

We first examined the adsorption geometries of hydrogen and glycerol on the Ru_4/ZrO_2 surface. It is well known that the dissociative adsorption of hydrogen on transition-metal surfaces is the first elementary step in a catalytic hydrogenation reaction. It has been found that reaction paths leading to dissociation of H_2 on metal surfaces proceed without or with very low barriers [38,39]. Accordingly, the initial structures of hy-



Scheme 1. Dehydration-hydrogenation reaction pathways (I and II) in glycerol hydrogenolysis to form propanediols.

drogen on the metal surface were assumed to be dissociated hydrogen atoms in this work. Similar modeling approaches have been successfully applied to various hydrogenation reactions on metal clusters or metal surfaces [40,41]. It should be noted that the adsorption configurations of glycerol on catalyst surfaces modify the final products; see Ref. [26] for details. If only the middle oxygen atom of the glycerol is linked to surface atoms, the final product is 1,2-PDO. In contrast, 1,3-PDO is obtained when two oxygen atoms are bonded with the catalyst. We therefore consider both plausible adsorption configurations as the starting conditions in the current work; see **2a** and **2a'** in Fig. 2. On structural relaxation, the adsorption of reactant **2a** is energetically favorable, with a calculated adsorption energy of -2.41 eV. The glycerol molecule is anchored to the top site of the Ru cluster through the O(2) atom of the middle hydroxyl group. The distance between Ru and O(2) is 0.229 nm. The adsorbed atomic hydrogen preferentially occupies the bridging Ru–Ru sites. This is a result of the lateral interactions between hydrogen atoms and the adsorbed glycerol on the Ru_4 cluster, suggesting that hydrogen atoms could move away from the stable three-fold site towards the bridging site. Preferential adsorption of hydrogen at the bridging site has also been observed theoretically using other metal surfaces or metal particles [40,41]. The formation of **2a'** is less favorable because it is located around 0.087 eV higher than **2a**. The primary hydroxyl O(1) atom sits on the top site of the Ru cluster and the secondary hydroxyl O(2) atom is positioned on the top site of Zr. The Ru–O(1) and Zr–O(2) bond lengths are 0.233 and 0.251 nm, respectively.

We next optimized the adsorption intermediates involved in the 1,2-PDO pathway, as shown in Fig. 2. In the first step, the

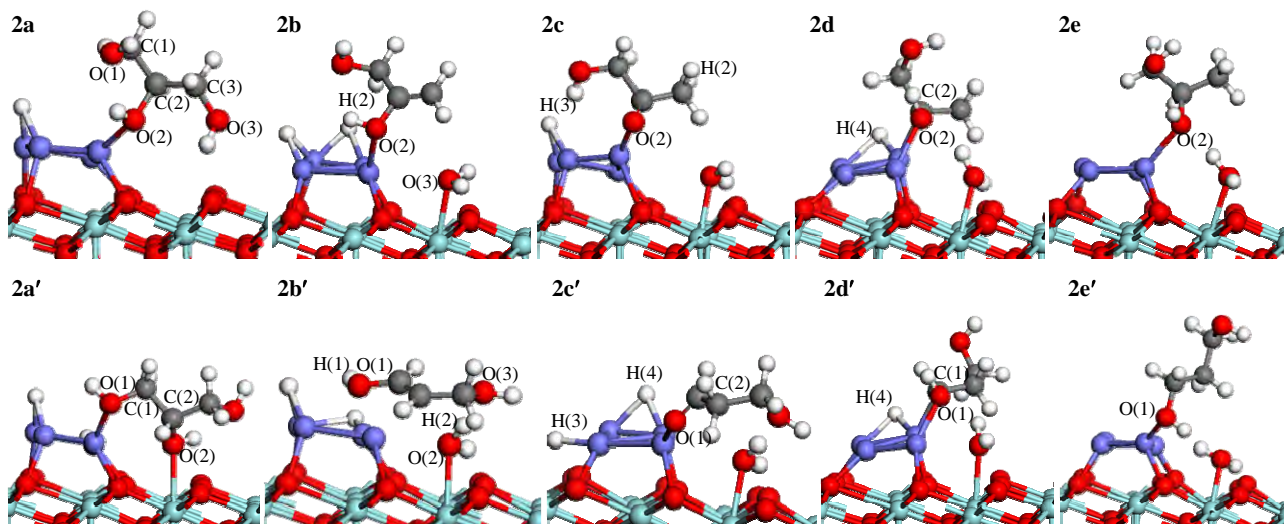


Fig. 2. Structures of intermediates for glycerol hydrogenolysis to 1,2-PDO (**2a–2e**) and 1,3-PDO (**2a'–2e'**) on $\text{Ru}_4/\text{ZrO}_2(111)$ surface.

propene-2,3-enol intermediate **2b** is formed via dehydration of the primary C(3)–O(3) bond and central C(2)–H bond. The secondary O(2) atom is pointing towards a Ru atom at a Ru–O(2) distance of 0.245 nm. The released water molecule prefers to sit on the top site of a lattice Zr, with a Zr–O(3) length of 0.232 nm. This step is modestly endothermic, by 0.43 eV. The 2,3-enol species can be further rearranged to the acetol intermediate **2c**, corresponding to the migration of the H(2) atom in **2b** to the C(3) fragment in **2c**. The surface adsorption of **2c** takes place on the top site of the Ru cluster through the keto O(2), which evolves a negative reaction energy of 1.05 eV. Then a H atom, H(3), adsorbed across the Ru₂ bridging site can combine with O(2) in **2c** to produce a semi-hydrogenated intermediate **2d**. The partially reduced intermediate adopts the bridged Ru₂ geometry via its central O(2)–C(2) bond in an exergonic process ($\Delta E = -0.26$ eV). The Ru–C(2) and Ru–O(2) bond lengths are 0.208 and 0.209 nm, respectively. In the last step, the Ru–C(2) bond is broken when the second H(4) atom moves towards the under-coordinated C(2) atom in **2d**, yielding an adsorbed 1,2-PDO species **2e**. The O(2) atom interacts with the metal cluster. The optimized Ru–O(2) distance is 0.235 nm. However, this step is heavily endothermic, with a reaction energy of 1.15 eV.

The first step on the path of 1,3-PDO formation converts **2a'** to the propene-1,3-enol intermediate **2b'** through breaking of the central C(2)–O(2) bond. During this reaction step, the Ru–O(1) bond is elongated ($d_{\text{Ru-O}} = 0.292$ nm), and the hydrogen bond between the O(3) atom of the 1,3-enol and the neighboring O(2)–H(2) group of the released water decreases to 0.165 nm. These results suggest an endothermic reaction of the 1,3-enol species, in agreement with the calculated reaction energy of 0.20 eV. The next step, the isomerization of the 1,3-enol intermediate to the adsorbed 3-hydroxypropanal species, is exothermic by -0.78 eV. A shift of H(1) occurs from O(1) in **2b'** to the C(2) atom in **2c'**, involving coordination of the carbonyl O(1) atom on the Ru cluster, which has a Ru–O(1) distance of 0.217 nm. In the subsequent step, coupling of one dissociated H(3) atom with the aldehyde O(1) atom to form an energetically favorable **2d'** species, Ru–C(1) and Ru–O(1) bonds are created with distances of 0.207 and 0.213 nm, respectively. This step has a reaction heat of -0.15 eV. In the final step, the second atomic H(4) attacks the unsaturated C(1) atom in **2d'** to give the adsorbed 1,3-PDO (**2e'**); the primary O(1) atom interacts closely with the Ru atom. This process is energetically difficult because of the positive reaction heat of 0.79 eV.

As illustrated in the potential energy profiles of these routes (Fig. 3), the relative stabilities of the primary C–O bond scission intermediates (**2a**, **2c**, and **2d**) are higher than the corresponding values for secondary C–O hydrogenolysis (**2a'**, **2c'**, and **2d'**). The energy difference reaches to 0.24 eV. The intermediate energies of **2b** and **2e** in the 1,2-PDO formation stage are comparable to those in the 1,3-PDO formation stage (**2b'** and **2e'**), with the energy difference being as small as 0.13 eV. Quantum mechanical calculations on the dehydration of neutral glycerol showed that the loss of a hydroxyl group from the terminal or central carbon, forming a propene-2,3-enol or pro-

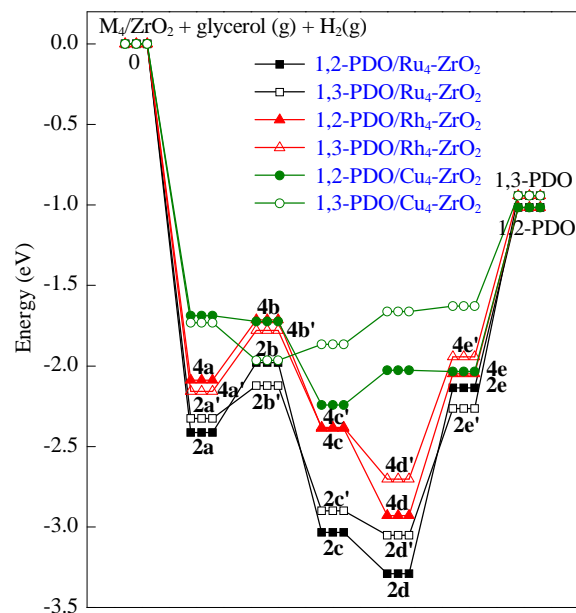


Fig. 3. Reaction profiles for glycerol hydrogenolysis on Ru₄/ZrO₂(111) and Rh₄/ZrO₂(111) surfaces. The zero energy is taken as the sum of the energies of M₄/ZrO₂(111), gas-phase glycerol, and gas-phase hydrogen. The energy diagram for glycerol hydrogenolysis on Cu₄/ZrO₂(111) reported in previous work is also shown for comparison.

pane-1,3-enol intermediate, have nearly equal energy barriers. However, in the subsequent keto-enol tautomerization, generation of hydroxyl acetone was more favorable than 3-hydroxypropanal formation [22]; this is in good agreement with our findings. Overall, 1,2-PDO is the thermodynamically preferred product and is favored under thermodynamic control. This might explain why on Ru catalysts the major product is 1,2-PDO.

3.3. Hydrogenolysis of glycerol on Rh₄/ZrO₂(111) surface: DFT studies

For comparison, we discuss the catalytic hydrogenolysis of glycerol on Rh₄/ZrO₂ surfaces. As illustrated in Fig. 4, the structures of the intermediates in the two routes to 1,2-PDO (**4a–4e**) and 1,3-PDO (**4a'–4e'**) over Rh₄/ZrO₂ are very similar to those of the corresponding stationary points over the Ru₄/ZrO₂ surface. The major difference between them is that one metal–O bond disappears for the final product, 1,3-PDO, on Rh₄/ZrO₂. In **4e'**, the strong attraction between the primary hydroxyl O(1) and the water H(2) atom causes movement of the O(1) atom away from the Rh atom.

The calculated energy diagrams of the two reaction pathways over Rh₄/ZrO₂ are presented in Fig. 3. For both the 1,2-PDO and 1,3-PDO routes, many key species, such as reactants (**4a** and **4a'**), products (**4e** and **4e'**), and some intermediates (**4b** and **4b'**, **4c** and **4c'**), are comparable energetically. However, the relative stability of the product after hydrogen transfer (**4d**) in the 1,2-PDO formation stage is much higher than that of the corresponding product **4d'** in the 1,3-PDO formation stage. The energy difference reaches 0.23 eV. Such a

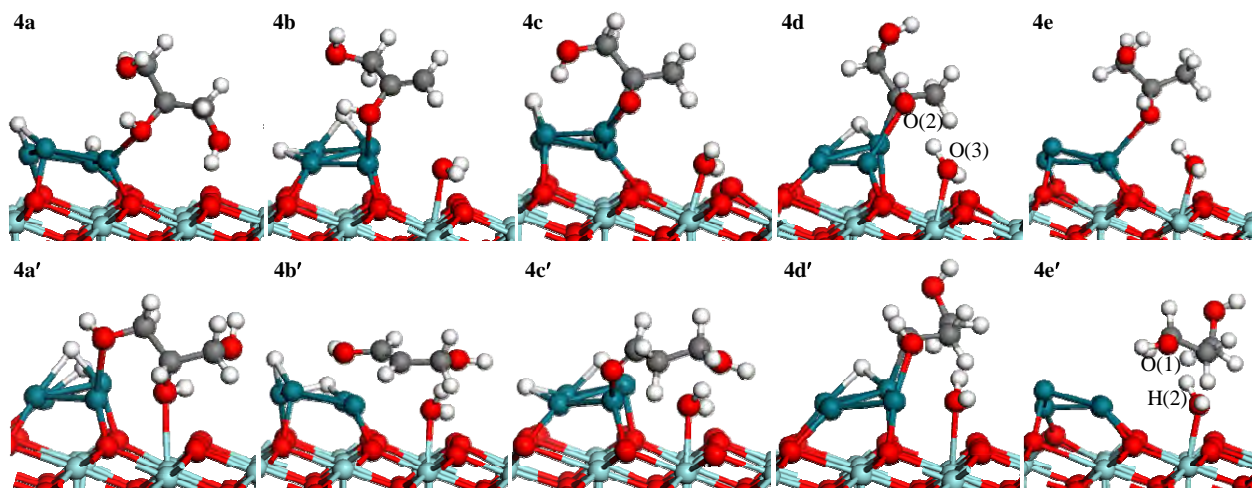


Fig. 4. Structures of intermediates for glycerol hydrogenolysis to 1,2-PDO (4a-4e) and 1,3-PDO (4a'-4e') on $\text{Rh}_4/\text{ZrO}_2(111)$ surface.

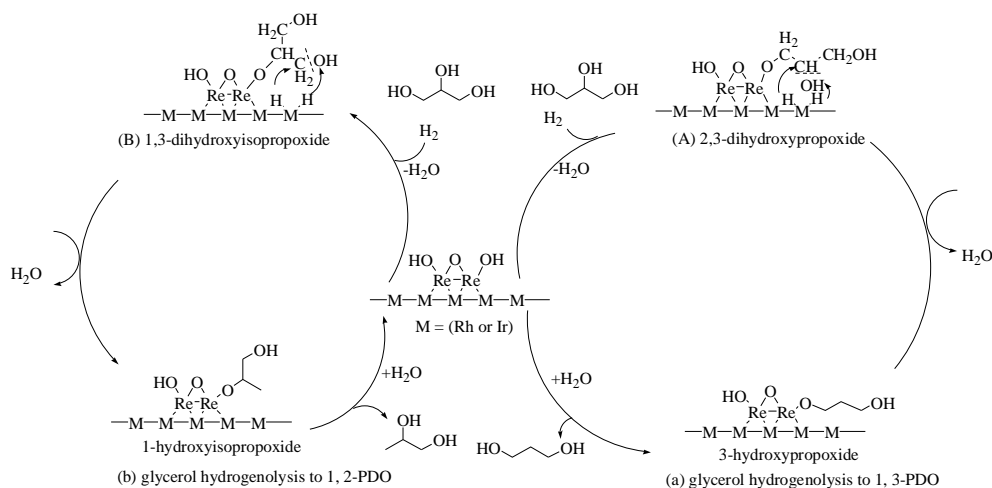
difference can be explained by the formation of a hydrogen bond, $\text{O}(3)\cdots\text{O}(2)$, in **4d**. 1,2-PDO is therefore favored under thermodynamic control. This finding is in line with the results on the Ru_4/ZrO_2 catalyst; see the previous section. It is also worthwhile comparing the performance of the current Rh_4/ZrO_2 catalyst with that of the Cu_4/ZrO_2 catalyst studied previously [26]. It is interesting to find that the 1,2-PDO path is even more easily accessible than the 1,3-PDO path for Cu_4/ZrO_2 . Note that the intermediate (acetol species) in such a case is very stable thermodynamically, being 0.39 eV lower in energy than 3-hydroxypropanal. We therefore suggest that excellent 1,2-PDO selectivity can be achieved on Cu catalysts. These findings are consistent with the experimental observations, which show that Cu catalysts have superior performance in terms of selectivity for 1,2-PDO. This also explains why other d9-metal-based catalysts (Ag) give nearly 100% selectivity for 1,2-PDO [42]. However, when noble metals (Ru, Rh) are involved, the selectivity decreases abruptly. The reason is that the high activity easily leads to cleavage of both C–C and C–O bonds.

As shown in Fig. 3, the relative stabilities of the intermediates are strongly dependent on the choice of transition-metal clusters, which could exert a large influence on the reaction

reactivity. The chemisorption energies of dehydrated and hydrogenated intermediates on Ru_4/ZrO_2 (**2a–2e**) are much lower than those on Rh_4/ZrO_2 (**4a–4e**). The difference is up to 0.36 eV, which suggests that Ru is more active than Rh for the hydrogenolysis of glycerol from the thermodynamics viewpoint. In addition, the binding energies of the structures on Cu are significantly higher than those of structures on Ru and Rh, indicating that Cu is the least active catalyst for the hydrogenolysis of glycerol. The reaction capabilities of the Ru-, Rh-, and Cu-based catalysts can be resolved by considering the density of states (DOS) around the Fermi level, as reported in Wang's work [43]. The Rh and Ru surfaces, which show a much delocalized DOS distribution near the Fermi level, can be regarded as more active catalysts for reactions. The Cu surface, in contrast, showing a more localized DOS distribution, is less active.

3.4. Hydrogenolysis of glycerol on $\text{Re}_2\text{O}_3\text{H}_2\text{-Rh}_4/\text{ZrO}_2(111)$: DFT studies

Scheme 2 shows model schemes for glycerol hydrogenolysis to 1,3-PDO and 1,2-PDO over $\text{Re}_2\text{O}_3\text{H}_2\text{-Rh}_4/\text{ZrO}_2$ and $\text{Re}_2\text{O}_3\text{H}_2\text{-Ir}_4/\text{ZrO}_2$ surfaces. The branching ratio to produce 1,2-PDO and 1,3-PDO is highly dependent on which hydroxyl



Scheme 2. Proposed mechanism for ReO_x -enhanced glycerol conversion and 1,3-PDO selectivity.

group is adsorbed first on the surface of the ReO_x cluster, and which one is cleaved in the subsequent hydride transfer step. When the primary CH_2OH group of glycerol is adsorbed on the ReO_x cluster, the formation of 2,3-dihydroxypropoxide (A) is achieved. Next, the middle C–O bond is broken by nucleophilic attack of hydrogen on the 2-position hydroxyl group of 2,3-dihydroxypropoxide to produce 3-hydroxypropoxide. Hydrolysis of 3-hydroxypropoxide releases the product, 1,3-PDO. In contrast, 1,2-PDO can be produced when glycerol is adsorbed at the middle C–OH bond to form 1,3-dihydroxyisopropoxide (B). The attack of the hydrogen atom at the 1-position of the C–O bond neighboring the C–ORe site gives 1-hydroxyisopropoxide. Hydrolysis of 1-hydroxyisopropoxide releases the product, 1,2-PDO.

As the initial state for 1,2-PDO formation over the $\text{Re}_2\text{O}_3\text{H}_2\text{-Rh}_4$ catalyst, we propose that glycerol is adsorbed on the $\text{Re}_2\text{O}_3\text{H}_2\text{-Rh}_4$ cluster to give two hydrogen-bonded configurations (Fig. 5, **5a**). The first is characterized by binding between the O(2) atom and the top of the terminal Re-O(4)H(4) , and the second configuration shows that the hydroxyl group O(1)–H(1) is pointing towards the bridging O(5) atom of the bimetallic cluster. The O(2)···H(4) and O(5)···H(1) distances are calculated to be 0.198 and 0.205 nm, respectively. The hydrogen atoms H(5) and H(6) lie on the bridging Rh–Rh and Rh–Re sites. The reaction is exothermic by -1.69 eV. In the subsequent step, dehydration occurs through O(2)–H(2) bond scission at the 2-position of glycerol and Re-O(4) bond cleavage of the modified cluster, leading to the formation of 1,3-dihydroxyisopropoxide species **5b**. Both the O(2) and O(3) atoms are adsorbed above the Re atom in a five-membered ring structure. The Re–O bond distances are 0.197 and 0.227 nm. Concurrently, hydrogen bonding is observed for the O(3)–H(3) group of 1,3-dihydroxyisopropoxide interacting with the released water O(4) atom located at the top site of the substrate surface. The reaction energy of this step is -0.048 eV. Next, the

H(5) atom activated on the Rh–Rh site attacks the O(3) atom of 1,3-dihydroxyisopropoxide to produce 2-oxetanemethanol **5c**, leading to breaking of the C(3)–O(3) bond and formation of a Re–C(3) bond arranged in a four-membered ring geometry. The optimized Re–C(3) and Re–O(2) bond lengths are 0.214 and 0.199 nm, respectively. The length of the newly formed Rh–O(3) bond is 0.229 nm and the reaction heat for 2-oxetanemethanol formation is -0.57 eV. Subsequently, the surface H(6) atom moves close to the under-coordinated C(3) atom in **5c**, giving rise to formation of 1-hydroxyisopropoxide **5d**, which is bound to the metal cluster via the Re–O(2) bond, with an energy gain of 0.043 eV. Finally, preferential hydrolysis of 1-hydroxyisopropoxide by the newly formed water molecule occurs. This leads to 1,2-PDO formation and the $\text{Re}_2\text{O}_3\text{H}_2\text{-Rh}_4$ recovers its initial state (**5e**). In this stable configuration, a hydrogen bond is formed between the O(2) atom in the secondary hydroxyl of 1,2-PDO and a neighboring hydrogen atom at the Re–Rh cluster. This step is calculated to be endothermic by 0.36 eV.

At the beginning of the process of 1,3-PDO formation over the $\text{Re}_2\text{O}_3\text{H}_2\text{-Rh}_4$ model system, the glycerol is located at the top of the cluster in a hydrogen-bond-like mode (**5a'**), in which the O(1) end of glycerol reacts with a vicinal hydrogen atom from Re-O(4)H(4) . For the dissociated hydrogens, one hydrogen atom, H(5), favors the bridging site of Rh–Rh, and the preferred adsorption site of another H(6) atom is the Rh–Re bridging site. The reaction energy of this step is -1.57 eV. This is followed by a condensation reaction between the O(1)–H(1) group of glycerol and a neighboring Re-O(4)H(4) , leading to the formation of the 2,3-dihydroxypropoxide intermediate **5b'**. The O(1) and O(2) atoms both bind to the Re atom, with Re–O distances of 0.202 and 0.223 nm, respectively. This step is slightly endothermic, by 0.091 eV. In the next step, H(5) moves from the Rh_2 bridging site to the O(2) atom of 2,3-dihydroxypropoxide. This results in cleavage of the C(2)–O(2) bond and formation of the

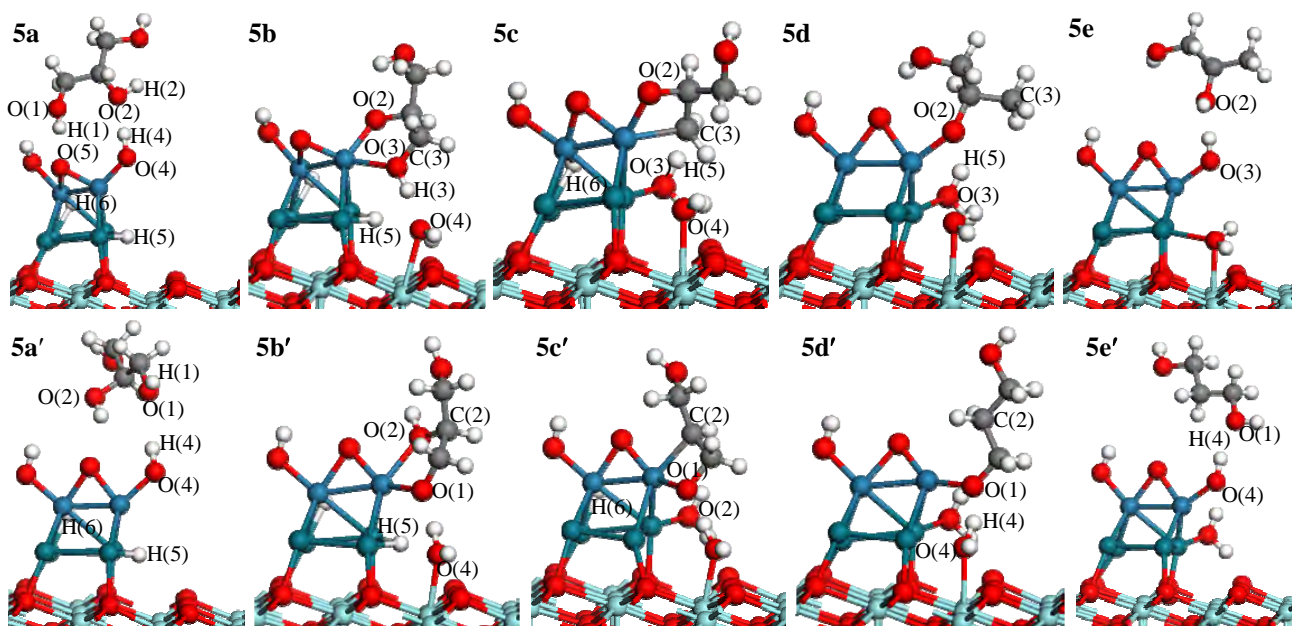


Fig. 5. Structures of intermediates for glycerol hydrogenolysis to 1,2-PDO (**5a**–**5e**) and 1,3-PDO (**5a'**–**5e'**) on $\text{Re}_2\text{O}_3\text{H}_2\text{-Rh}_4/\text{ZrO}_2(111)$ surface.

3-oxetanemethanol intermediate **5c'**, which easily binds to the Re atom through Re–C(2) (0.218 nm) and Re–O(1) (0.200 nm) bonds. The newly formed water molecule binds to a Rh atom with a Rh–O(2) bond length of 0.225 nm. This step exhibits a reaction heat as high as -0.50 eV. Next, the insertion of another H(6) atom at the unsaturated C(2) atom in **5c'** competes for the 3-hydroxypropoxide species **5d'**, which stays at the top site of Re, with an Re–O(1) bond length of 0.199 nm. A hydrogen bond (0.147 nm) originating from interaction of the alkoxide O(1) atom with the O(4)–H(4) group of water is observed. This process is expected to be exothermic by -0.035 eV. The Re–O(1) bond is dissociated when the water molecule binding at the Rh site moves towards the Re atom, yielding an adsorbed 1,3-PDO species **5e'**. The primary O(1) atom of the 1,3-PDO species prefers to point to the terminal Re–O(4)H(4) of the bimetallic cluster, forming a hydrogen-bond-like structure with an O(1)⋯H(4) length of 0.175 nm. Our calculations give a positive reaction energy of 0.44 eV associated with this process.

From the results of the DFT-calculated energies in Fig. 6, we can conclude that the catalyst exhibits a slight preference for adsorption of the intermediates responsible for 1,2-PDO formation. This is in agreement with the experimental selectivity, since 1,2-PDO remains the major product on $\text{Re}_2\text{O}_3\text{H}_2\text{-Rh/SiO}_2$. However, it is interesting to note that each stationary point on the 1,3-PDO route is only a little higher in energy than the counterpart on the 1,2-PDO route. For example, the adsorbed 3-oxetanemethanol **5c'**, which leads to 1,3-PDO, is 0.14 eV energetically less stable than 2-oxetanemethanol **5c**, which yields 1,2-PDO. The binding energies differ slightly along the 1,2-PDO and 1,3-PDO pathways for other key species such as the reactants (**5a** and **5a'**) and alkoxide species (**5b** and **5b'**, **5d** and **5d'**), with the value being as small as 0.065 eV, indicating that the formation of 1,3-PDO is competitive with the formation of 1,2-PDO from a thermodynamics viewpoint. The stability order of the precursors might explain why a small fraction of 1,3-PDO is obtained experimentally on the Re-modified Rh catalyst.

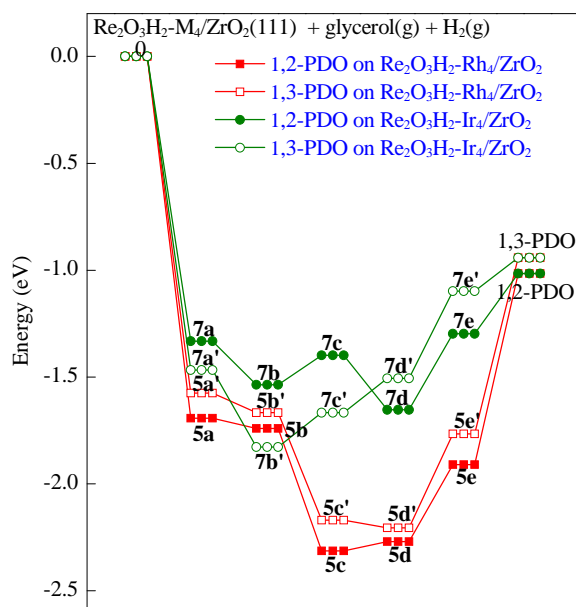


Fig. 6. Reaction profiles for glycerol hydrogenolysis on $\text{Re}_2\text{O}_3\text{H}_2\text{-Rh}_4/\text{ZrO}_2(111)$ and $\text{Re}_2\text{O}_3\text{H}_2\text{-Ir}_4/\text{ZrO}_2(111)$. The zero energy is taken as the sum of the energies of $\text{Re}_2\text{O}_3\text{H}_2\text{-M}_4/\text{ZrO}_2(111)$, gas-phase glycerol, and gas-phase hydrogen.

3.5. Hydrogenolysis of glycerol on $\text{Re}_2\text{O}_3\text{H}_2\text{-Ir}_4/\text{ZrO}_2(111)$: DFT studies

The most favorable structures of the intermediates for glycerol hydrogenolysis over $\text{Re}_2\text{O}_3\text{H}_2\text{-Ir}_4/\text{ZrO}_2$ are depicted in Fig. 7. One can clearly see that most of the optimized geometries of the intermediates are very close to the corresponding stationary points on the $\text{ReO}_x\text{-Rh}/\text{ZrO}_2$ surface. The major difference between them lies in the locations of the H(5) and H(6) atoms in the starting structures. The top of the Ir cluster is found to be the most favorable binding site for breaking H(5) and H(6)

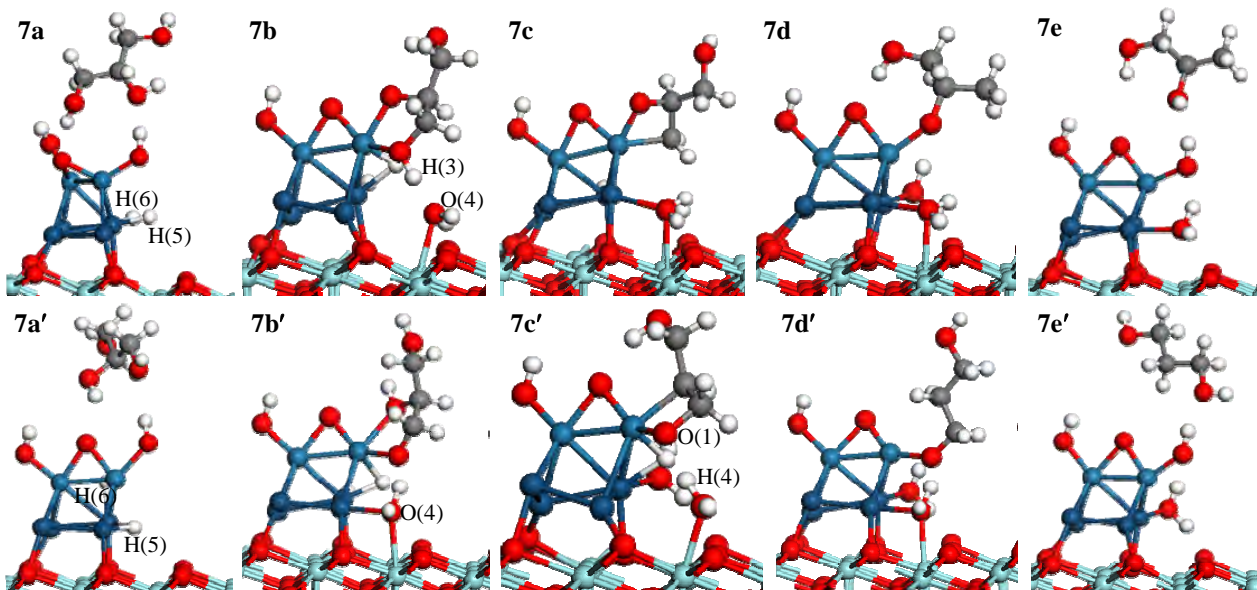


Fig. 7. Structures of intermediates for glycerol hydrogenolysis to 1,2-PDO (**7a–7e**) and 1,3-PDO (**7a'–7e'**) on $\text{Re}_2\text{O}_3\text{H}_2\text{-Ir}_4/\text{ZrO}_2(111)$ surface.

atoms for **7a**, whereas the Rh–Rh and Rh–Re bridging sites are preferred for **5a**.

Figure 6 gives the energetics associated with these two routes on the Re-modified Ir catalyst. It can immediately be seen that the adsorbed intermediates responsible for 1,3-PDO formation (**7a'**, **7b'**, and **7c'**) are more stable than the corresponding isomers responsible for 1,2-PDO (**7a**, **7b**, and **7c**). The adsorbed 2,3-dihydroxypropoxide **7b'**, for example, is 0.29 eV lower in energy than the adsorbed 1,3-dihydroxyisopropoxide **7b**. Such a difference can be rationalized by the creation of a new Ir–O(4) bond in **7b'**. In addition, the adsorbed 3-oxetanemethanol **7c'** is 0.27 eV more stable than the adsorbed 2-oxetanemethanol **7c**. The extra stability of **7c'** could be caused by the formation of a hydrogen bond, O(4)–H(4)···O(1). In the absence of activation energy barriers, or under equilibrium conditions, these increased stabilities of the 1,3-PDO intermediates would ensure higher surface coverage by 1,3-PDO. Such a conclusion agrees well with the experimental results obtained by Nakagawa and coworkers [18], which showed that the selectivity for 1,3-PDO is greatly enhanced when the catalyst is changed from Re-modified Rh to Re-modified Ir, as reflected in the 1,3-PDO to 1,2-PDO ratio.

Clearly, a steric effect for preferential terminal alkoxide formation is induced by the large atomic radius of Ir, which may be the key to the high 1,3-PDO selectivity on Re-doped Ir catalysts. Glycerol has two coordination modes when it is adsorbed on Re species. The 2,3-dihydroxypropoxide intermediate resulting from condensation between the primary hydroxyl group and the $\text{Re}_2\text{O}_3\text{H}_2\text{-Ir}_4$ cluster is stable, whereas the 1,3-dihydroxyisopropoxide intermediate requires a large adsorption cross-section. The same behavior has been reported in the esterification of Nb- or V-substituted polyoxotungstates with alcohols. Steric crowding resulting from the introduction of a secondary carbon center at the bridging oxygen site was observed in the presence of secondary alcohols but was absent in the case of methanol [44,45]. In contrast to the kinetically favorable formation of 1,3-PDO on $\text{Re}_2\text{O}_3\text{H}_2\text{-Ir}_4$, the growth of Rh–Re clusters on the Re-modified Rh catalyst is not large enough to induce a significant difference between the stabilities of the terminal metal alkoxide species and the secondary alkoxides species. In other words, elimination of the primary hydroxyl group to form 1,2-PDO competes with deoxygenation of the secondary hydroxyl group to form 1,3-PDO.

As shown in Fig. 6, the calculated adsorption energies of the intermediates for 1,3-PDO formation on $\text{Re}_2\text{O}_3\text{H}_2\text{-Rh}_4/\text{ZrO}_2$ (**5a'–5e'**) are stronger than those of **7a'–7e'** on $\text{Re}_2\text{O}_3\text{H}_2\text{-Ir}_4/\text{ZrO}_2$. The energy difference is up to 0.78 eV; accordingly, the overall reactivity of the conversion of glycerol on Rh–Re is much higher than that on Ir–Re. The observed stabilities of the alkoxide structures might be attributable to the acidities of the hydroxylated Re species on the Rh–Re and Ir–Re catalysts, because Re–OH ligands are critical for the formation of metal alkoxides. The hydroxylated Re species on the $\text{Re}_2\text{O}_3\text{H}_2\text{-Rh}$ cluster have deprotonation energies of 3.4 eV, compared with a value of 3.9 eV for the $\text{Re}_2\text{O}_3\text{H}_2\text{-Ir}_4$ cluster. It is therefore evident that the DFT-predicted acidities of the hydroxylated Re species on Rh–Re are significantly stronger than those for Ir–Re,

consistent with the stronger adsorption of alkoxide intermediates observed for glycerol over $\text{Re}_2\text{O}_3\text{H}_2\text{-Rh}_4$.

Experimental observations for glycerol hydrogenolysis on Re-modified catalysts showed that the catalytic activities, compared with those of monometallic catalysts, were greatly enhanced by the addition of Re [17]. The higher activity of the Rh–Re system is consistent with the premise that a direct hydrogenolysis mechanism would be displayed as a result of Re modification, whereas monometallic Rh is only capable of facilitating indirect hydrogenolysis. It has been suggested that the formation of terminal alkoxide species is essential for the selective hydrogenolysis of glycerol to 1,3-PDO. The development of novel catalysts to stabilize the adsorption states of terminal alkoxide intermediates is desirable for achieving high yields of 1,3-PDO.

4. Conclusions

Periodic DFT calculations with the GGA-PW91 functional were used to study the thermochemistry of the elementary steps for glycerol hydrogenolysis on ZrO_2 -supported Ru_4 , Rh_4 , $\text{Re}_2\text{O}_3\text{H}_2\text{-Rh}_4$, and $\text{Re}_2\text{O}_3\text{H}_2\text{-Ir}_4$ catalysts. The decisive role of ReO_x present in the Re-modified Rh and Ir bifunctional catalysts in modifying the activity and 1,3-PDO selectivity during glycerol hydrogenolysis was illustrated.

The DFT results suggest that the decomposition pathways on Ru_4/ZrO_2 and Rh_4/ZrO_2 may proceed through a dehydration-hydrogenation mechanism. The primary or secondary C–O bond of glycerol is initially dehydrated, followed by hydrogenation to give 1,2-PDO or 1,3-PDO. For the two reaction routes considered here, facial formation of 1,2-PDO was observed as a result of the stronger binding of acetol isomers compared with 3-hydroxypropanal. Compared with those of Cu catalysts, the activity towards 1,2-PDO can be greatly enhanced by using Ru and Rh catalysts, although the selectivity becomes lower.

A direct hydrogenolysis mechanism is proposed on the Re-modified Rh and Ir catalysts. The primary or secondary oxygen atom of glycerol is initially anchored to hydroxylated Re species. This gives an alkoxide, and then hydride transfer takes place to form 1,2-PDO or 1,3-PDO. In the case of a $\text{Re}_2\text{O}_3\text{H}_2$ -doped Rh catalyst, the growth of Rh–Re clusters is not sufficiently large to induce significant differences between the stabilities of the terminal alkoxide and secondary alkoxides species. Consequently, deoxygenation of the secondary C–O bond to form 1,3-PDO becomes competitive with elimination of the primary hydroxyl group to form 1,2-PDO. The 1,3-PDO selectivity is further improved by using Re-promoted Ir/ZrO_2 , as a result of the large atomic radius of Ir. Binding of the terminal alkoxide on the surface is much stronger than that of its secondary alkoxide counterpart. It turns out that the formation of sterically preferred terminal alkoxide species may be the key to the high 1,3-PDO selectivity on the modified catalysts compared with the case of indirect hydrogenolysis on monometallic catalysts.

As the first step towards understanding the performance of Re-modified bifunctional catalysts, we performed a detailed thermochemical analysis of the reaction mechanisms. Although

Graphical Abstract

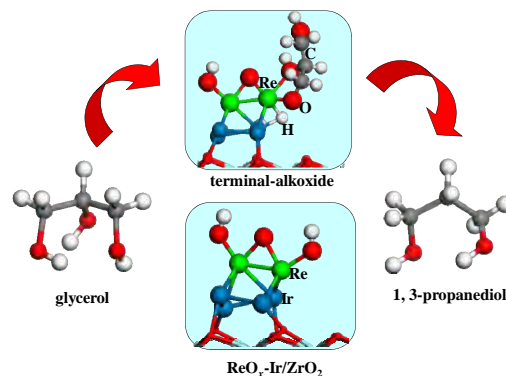
Chin. J. Catal., 2013, 34: 1656–1666 doi: 10.1016/S1872-2067(12)60626-3

Role of ReO_x in Re-modified Rh/ ZrO_2 and Ir/ ZrO_2 catalysts in glycerol hydrogenolysis: insights from first-principles study

Jing Guan, Xiufang Chen, Gongming Peng, Xicheng Wang, Quan Cao, Zhenggang Lan*, Xindong Mu*

Qingdao Institute of Bioenergy and Bioprocess Technology, Chinese Academy of Sciences

The decisive role of ReO_x present in Re-modified bifunctional catalysts in promoting the activity and 1,3-propanediol selectivity, compared with monometallic clusters, is highlighted.



the results of this approach are rather preliminary, our findings here are consistent with previous experimental observations. We believe that the mechanistic insights from this work are reasonable and will motivate further theoretical and experimental studies on the selective hydrogenolysis of glycerol. A more accurate understanding of this issue requires an explicit kinetic analysis of activation energy barriers, transition states, and even the computational accuracy (using large metal nanoparticles and the inclusion of a solvent effect in the model). Such a kinetic analysis is a great challenge because of the system complexity, the uncertainty associated with multiple components, and the various reaction mechanisms. This will be the subject of future research.

Acknowledgments

The authors thank Super Computing Center, Computer Network Information Center, CAS for providing computational resources.

References

- [1] Werpy T, Petersen G. Top Value Added Chemicals from Biomass. Volume I: Results of Screening for Potential Candidates from Sugars and Synthesis Gas. US DOE Report, 2004
- [2] Nakagawa Y, Tomishige K. *Catal Sci Technol*, 2011, 1: 179
- [3] Huang Z W, Cui F, Kang H X, Chen J, Zhang X Z, Xia C G. *Chem Mater*, 2008, 20: 5090
- [4] Chaminand J, Djakovitch L, Gallezot P, Marion P, Pinel C, Rosier C. *Green Chem*, 2004, 6: 359
- [5] Dasari M A, Kiatsimkul P P, Sutterlin W R, Suppes G J. *Appl Catal A*, 2005, 281: 225
- [6] Werpy T A, Frye G Jr, Zacher A H, Miller D J. US Patent 6 841 085. 2005
- [7] Perosa A, Tundo P. *Ind Eng Chem Res*, 2005, 44: 8535
- [8] Lahr D G, Shanks B H. *J Catal*, 2005, 232: 386
- [9] Miyazawa T, Kusunoki Y, Kunimori K, Tomishige K. *J Catal*, 2006, 240: 213
- [10] Miyazawa T, Koso S, Kunimori K, Tomishige K. *Appl Catal A*, 2007, 329: 30
- [11] Feng J, Fu H Y, Wang J B, Li R X, Chen H, Li X J. *Catal Commun*, 2008, 9: 1458
- [12] Kurosaka T, Maruyama H, Naribayashi I, Sasaki Y. *Catal Commun*, 2008, 9: 1360
- [13] Maris E P, Ketchie W C, Murayama M, Davis R J. *J Catal*, 2007, 251: 281
- [14] Ma L, Li Y M, He D H. *Chin J Catal* (马兰, 李宇明, 贺德华. 催化学报), 2011, 32: 872
- [15] Liu L J, Zhang Y H, Wang A Q, Zhang T. *Chin J Catal* (刘龙杰, 张艳华, 王爱琴, 张涛. 催化学报), 2012, 33: 1257
- [16] Shimao A, Koso S, Ueda N, Shinmi Y, Furikado I, Tomishige K. *Chem Lett*, 2009, 38: 540
- [17] Shinmi Y, Koso S, Kubota T, Nakagawa Y, Tomishige K. *Appl Catal B*, 2010, 94: 318
- [18] Nakagawa Y, Shinmi Y, Koso S, Tomishige K. *J Catal*, 2010, 272: 191
- [19] Deniel O M, DeLaRiva A, Kunkes E L, Datye A K, Dumesic J A, Davis R J. *ChemCatChem*, 2010, 2: 1107
- [20] Montassier C, Giraud D, Barbier J. *Stud Surf Sci Catal*, 1988, 41: 165
- [21] Montassier C, Menezes J C, Hoang L C, Renaud C, Barbier J. *J Mol Catal*, 1991, 70: 99
- [22] Nimlos M R, Blanksby S J, Qian X H, Himmel M E, Johnson D K. *J Phys Chem A*, 2006, 110: 6145
- [23] Auneau F, Michel C, Delbecq F, Pinel C, Sautet P. *Chem Eur J*, 2011, 17: 14288
- [24] Coll D, Delbecq F, Aray Y, Sautet P. *Phys Chem Chem Phys*, 2011, 13: 1448
- [25] Chia M, Pagan-Torres Y J, Hibbitts D, Tan Q H, Pham H N, Datye A K, Neurock M, Davis R J, Dumesic J A. *J Am Chem Soc*, 2011, 133: 12675
- [26] Guan J, Wang X C, Wang X Y, Mu X D. *Sci China Chem*, 2013, 56: 763
- [27] Kresse G, Joubert D. *Phys Rev B*, 1999, 59: 1758
- [28] Kresse G, Furthmueller J. *Phys Rev B*, 1996, 54: 11169
- [29] Kresse G, Hafner J. *Phys Rev B*, 1994, 49: 14251
- [30] Blöchl P E. *Phys Rev B*, 1994, 50: 17953
- [31] Perdew J P, Wang Y. *Phys Rev B*, 1992, 45: 13244
- [32] Monkhorst H J, Pack J D. *Phys Rev B*, 1976, 13: 5188
- [33] Grau-Crespo R, Hernández N C, Sanz J F, DeLeeuw N H. *J Phys Chem C*, 2007, 111: 10448
- [34] Yang Z X, Xie L G, Ma D W, Wang G T. *J Phys Chem C*, 2011, 115: 6730
- [35] Pan Y X, Liu C J, Ge Q F. *J Catal*, 2010, 272: 227
- [36] Li H J, Ho J J. *J Phys Chem C*, 2009, 113: 20139
- [37] Chen H L, Peng W T, Ho J J, Hsieh H M. *Chem Phys*, 2008, 348: 161
- [38] Olsen R A, Kroes G J, Baerends E J. *J Chem Phys*, 1999, 111: 11155
- [39] German E D, Efremenko I, Sheintuch M. *J Phys Chem A*, 2001, 105: